

The following resources related to this article are available online at www.sciencemag.org (this information is current as of October 16, 2009):

Updated information and services, including high-resolution figures, can be found in the online version of this article at:

<http://www.sciencemag.org/cgi/content/full/325/5940/605>

Supporting Online Material can be found at:

<http://www.sciencemag.org/cgi/content/full/325/5940/605/DC1>

A list of selected additional articles on the Science Web sites **related to this article** can be found at:

<http://www.sciencemag.org/cgi/content/full/325/5940/605#related-content>

This article **cites 28 articles**, 6 of which can be accessed for free:

<http://www.sciencemag.org/cgi/content/full/325/5940/605#otherarticles>

This article has been **cited by** 1 articles hosted by HighWire Press; see:

<http://www.sciencemag.org/cgi/content/full/325/5940/605#otherarticles>

This article appears in the following **subject collections**:

Geochemistry, Geophysics

http://www.sciencemag.org/cgi/collection/geochem_phys

Information about obtaining **reprints** of this article or about obtaining **permission to reproduce this article** in whole or in part can be found at:

<http://www.sciencemag.org/about/permissions.dtl>

17. P. C. Clark, S. C. O. Glover, R. S. Klessen, *Astrophys. J.* **672**, 757 (2008).
18. M. N. Machida, K. Omukai, T. Matsumoto, S.-i. Inutsuka, *Astrophys. J.* **677**, 813 (2008).
19. V. Bromm, P. S. Coppi, R. B. Larson, *Astrophys. J.* **527**, L5 (1999).
20. B. W. O'Shea *et al.*, in *Adaptive Mesh Refinement: Theory and Applications*, T. Plewa, T. Linde, G. Weirs, Eds. (Springer-Verlag, Berlin, 2004).
21. Detailed simulation parameters and methods are available as supporting material on Science Online.
22. N. Yoshida, T. Abel, L. Hernquist, N. Sugiyama, *Astrophys. J.* **592**, 645 (2003).
23. E. C. Ostriker, *Astrophys. J.* **513**, 252 (1999).
24. K. Omukai, Y. Yoshii, *Astrophys. J.* **599**, 746 (2003).
25. I. Hachisu, J. E. Tohline, Y. Eriguchi, *Astrophys. J. Suppl. Ser.* **66**, 315 (1988).
26. I. Hachisu, J. E. Tohline, Y. Eriguchi, *Astrophys. J.* **323**, 592 (1987).
27. T. Abel, J. H. Wise, G. L. Bryan, *Astrophys. J.* **659**, L87 (2007).
28. J. Tumlinson, *Astrophys. J.* **641**, 1 (2006).
29. B. W. O'Shea, T. Abel, D. Whalen, M. L. Norman, *Astrophys. J.* **628**, L5 (2005).
30. J. H. Wise, T. Abel, *Astrophys. J.* **685**, 40 (2008).
31. B. W. O'Shea, M. L. Norman, *Astrophys. J.* **673**, 14 (2008).
32. We thank V. Bromm, G. Bryan, A. Escala, S. Glover, C. McKee, J. Oishi, B. Smith, J. Tumlinson, and N. Yoshida for useful discussions. This work was partially supported by the U.S. Department of Energy (DOE) contract to Stanford Linear Accelerator Center no. DE-AC02-76SF00515, NASA Astrophysics Theory and Fundamental Physics grant NNX08AH26G, and NSF AST-0807312. B.W.O. and M.J.T.

carried out this work in part under the auspices of the National Nuclear Security Administration of the DOE at Los Alamos National Laboratory (LANL) under contract no. DE-AC52-06NA25396. B.W.O. was partially supported by a LANL Director's Postdoctoral Fellowship (DOE LDRD grant 20051325PRD4).

Supporting Online Material

www.sciencemag.org/cgi/content/full/1173540/DC1
Materials and Methods
Table S1
References

13 March 2009; accepted 15 June 2009
Published online 9 July 2009;
10.1126/science.1173540
Include this information when citing this paper.

Water and the Oxidation State of Subduction Zone Magmas

Katherine A. Kelley^{1,†} and Elizabeth Cottrell^{2,*}

Mantle oxygen fugacity exerts a primary control on mass exchange between Earth's surface and interior at subduction zones, but the major factors controlling mantle oxygen fugacity (such as volatiles and phase assemblages) and how tectonic cycles drive its secular evolution are still debated. We present integrated measurements of redox-sensitive ratios of oxidized iron to total iron ($\text{Fe}^{3+}/\Sigma\text{Fe}$), determined with Fe K-edge micro-x-ray absorption near-edge structure spectroscopy, and pre-eruptive magmatic H_2O contents of a global sampling of primitive undegassed basaltic glasses and melt inclusions covering a range of plate tectonic settings. Magmatic $\text{Fe}^{3+}/\Sigma\text{Fe}$ ratios increase toward subduction zones (at ridges, 0.13 to 0.17; at back arcs, 0.15 to 0.19; and at arcs, 0.18 to 0.32) and correlate linearly with H_2O content and element tracers of slab-derived fluids. These observations indicate a direct link between mass transfer from the subducted plate and oxidation of the mantle wedge.

Plate tectonics leads to a two-way geochemical exchange between Earth's interior and exterior. This process is driven by the formation of new oceanic crust by mantle melting at mid-ocean ridges, hydration and oxidative alteration of oceanic crust as it transits the seafloor, and the subsequent return of hydrated oxidized oceanic crust to the deep Earth at subduction zones (Fig. 1A) (1, 2). How this exchange has affected the oxygen fugacity of the mantle spatially (3) and over time (2, 4, 5) remains unclear. Many lines of evidence point to oxidizing conditions in arc peridotites and magmas (1, 6), but a quantitative link between oxidation state and the subduction process, although intuitive, has not been established. Here we provide coupled measurements of the redox-sensitive $\text{Fe}^{3+}/\Sigma\text{Fe}$ ratio and magmatic H_2O concentrations at the same spatial resolution in a global suite of undegassed basaltic glasses, in order to determine the current oxidation condition of the mantle as a function of tectonic regime.

The ratio of oxidized iron to total iron [$\text{Fe}^{3+}/\Sigma\text{Fe} = \text{Fe}^{3+}/(\text{Fe}^{3+} + \text{Fe}^{2+})$] in primary, mantle-derived ba-

saltic melts reflects mantle oxygen fugacity, provided that magmas experience minimal modification as they ascend to the surface (1, 6–8). Melts may, however, be oxidized by crustal assimilation, crystallization, or degassing during ascent (3, 8, 9). Interpretation of bulk measurements of $\text{Fe}^{3+}/\Sigma\text{Fe}$ ratios in lavas (for example, by wet chemistry or Mössbauer spectroscopy) can be complicated because many rock samples, even at small scales, are mixtures of crystals and glass that may not represent true magmatic liquids. Lavas erupted on land also extensively degas, which alters their primary $\text{Fe}^{3+}/\Sigma\text{Fe}$ ratios (9). Submarine pillow rim glasses and melt inclusions (Fig. 1), however, can preserve primitive, minimally degassed magmatic liquids (10, 11).

We used synchrotron-based Fe K-edge micro-x-ray absorption near-edge structure (μ -XANES) spectroscopy to derive $\text{Fe}^{3+}/\Sigma\text{Fe}$ ratios from the valence-sensitive pre-edge feature corresponding to the $1s \rightarrow 3d$ electronic transition (12). The area-weighted average energy of the baseline-subtracted pre-edge feature (the centroid) shifts in energy as a function of Fe oxidation state in basaltic glass (13) (Fig. 2A). Natural basalt powders were equilibrated over 16 oxygen fugacities, between -3.5 and $+4.5$ log units relative to the quartz-fayalite-magnetite (QFM) buffer, to create a suite of calibration glasses of known $\text{Fe}^{3+}/\Sigma\text{Fe}$ ratios, independently determined by Mössbauer spectros-

copy (14). Over this compositional range, neither H_2O content (15) nor basalt major or minor element concentrations (14) influence the relation between the energy of the area-weighted centroid and $\text{Fe}^{3+}/\Sigma\text{Fe}$. These reference glasses can be used to extract the $\text{Fe}^{3+}/\Sigma\text{Fe}$ ratio of basalts from multiple tectonic settings and with varying H_2O content, with a precision of ± 0.0045 , comparable to that determined by wet chemistry (14).

Our samples represent melts from a range of tectonic settings, including global submarine pillow-rim glasses from primitive [>6 weight percent (wt %) MgO] mid-ocean ridge basalts (MORBs) and Mariana Trough back-arc basin basalts (BABBs), as well as basaltic olivine-hosted melt inclusions from one MORB and a global suite of arc volcanoes (Fig. 1) (12). Based on μ -XANES spectral

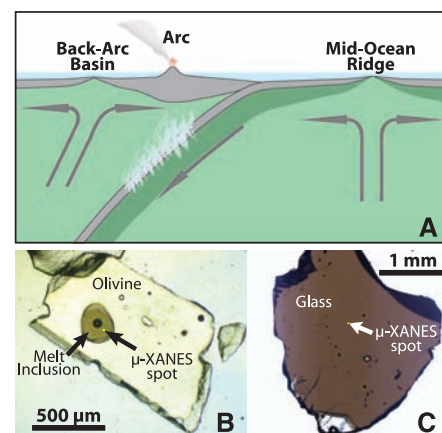


Fig. 1. (A) Cartoon showing plate tectonic settings of samples analyzed in this study. Mid-ocean ridges create oceanic crust through mantle upwelling. Hydrated and altered mid-ocean ridge crust is returned to the mantle by subduction, where H_2O released by metamorphic reactions enters the mantle sources of arc volcanoes and back-arc basins. (B) Photomicrograph of a double-polished, olivine-hosted arc melt inclusion (sample GUG-DB). The melt inclusion is originally glassy, free of daughter crystals, and contains a single vapor bubble caused by the contraction of the glass upon cooling. The size of the μ -XANES beam is shown for reference. (C) Photomicrograph of a wafered back-arc basin glass chip (sample ALV1839-21).

¹Graduate School of Oceanography, University of Rhode Island, Narragansett, RI 02882, USA. ²National Museum of Natural History, Smithsonian Institution, Washington, DC 20560, USA.

*These authors contributed equally to this work.

†To whom correspondence should be addressed. E-mail: kelley@gso.uri.edu

analysis, the $\text{Fe}^{3+}/\Sigma\text{Fe}$ ratio increases from the MORB (0.13 to 0.17) to BABB (0.15 to 0.19) to arc samples (0.18 to 0.32 (Fig. 2B and table S1), which is consistent with evidence that arc magmas are more oxidized than MORBs (1, 6) and contrary to models based on V/Sc ratios (3).

Pre-eruptive magmatic concentrations of volatiles (such as H_2O) are also known to vary with tectonic setting, and specifically to increase at subduction zones (10, 11). New measurements of the dissolved H_2O , CO_2 , and S concentrations of basaltic glasses were also conducted, either by ion microprobe, following the methods of Hauri (16), or by Fourier transform infrared spectroscopy (FTIR) and electron microprobe, using the methods of Luhr (10), and were used in conjunction with previously published volatile data (12). These results show that magmatic H_2O content increases from MORBs (0.14 to 0.49 wt %) to BABBs (0.57 to 1.89 wt %) to arcs [2.23 to 5.39 wt %; except in one sample from an arc volcano that is known to be H_2O -poor (17)]. The oxidation state of Fe in the basaltic melts increases linearly with magmatic H_2O concentrations (Fig. 3). The high H_2O contents of subduction zone magmas have long been expected to relate to oxidized magmas and mantle sources (1, 6, 18), but these data provide a direct quantitative correlation between $\text{Fe}^{3+}/\Sigma\text{Fe}$ and water content in global basaltic melts. If the movement of volatiles from the subducted plate into the arc mantle can be linked to changes in Fe oxidation state, then the subduc-

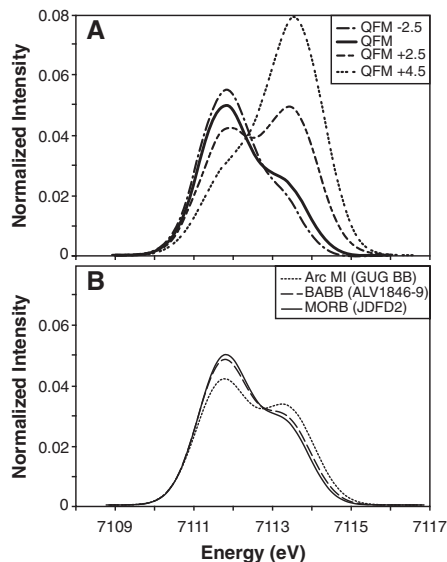


Fig. 2. Comparison of edge-step-normalized, baseline-subtracted, pre-edge μ -XANES spectra for basaltic glasses. The relative intensities of the two pre-edge peaks are diagnostic of the oxidation state of Fe in the glass. (A) Baseline-subtracted spectra for reference glasses of All-92-29-1 (12), equilibrated at QFM -2.5 (dash-dot line), QFM (solid line), QFM $+2.5$ (dash-double-dot line), and QFM $+4.5$ (triple-dot line). (B) Baseline-subtracted spectra for natural samples, including a MORB glass (JDFD2, thin solid line), a BABB glass (ALV1846-9, thin dashed line), and an arc melt inclusion (GUG BB, thin dotted line).

tion process may play a central role in changing the mantle oxygen fugacity both across modern tectonic settings and throughout Earth history.

Shallow magmatic processes could cause linear correlations between $\text{Fe}^{3+}/\Sigma\text{Fe}$ ratios and H_2O concentrations that are unrelated to the properties of the mantle source. Melt oxidation could occur through losses of some S species (such as H_2S) and H_2 driven by degassing or diffusion (8), but this would create an inverse relation between volatile content (such as H_2O) and $\text{Fe}^{3+}/\Sigma\text{Fe}$ ratio. We also excluded glasses showing evidence of H_2O degassing (low concentrations of earlier-degassing CO_2 or S). Small increases in $\text{Fe}^{3+}/\Sigma\text{Fe}$ ratios and H_2O contents are expected (and are observed within the MORB glasses) because Fe^{3+} and H_2O are incompatible in early-crystallizing olivine, whereas Fe^{2+} is compatible. The trajectories of both $\text{Fe}^{3+}/\Sigma\text{Fe}$ ratios and H_2O concentrations relative to MgO content, however, indicate that olivine fractional crystallization cannot explain the observed relation between Fe oxidation state and H_2O in BABBs and arc glasses. The melt inclusion samples could also have been modified by post-entrapment crystallization of olivine or diffusive loss of Fe^{2+} . Both of these processes can be detected, and the compositions can be corrected through analysis of melt compositions relative to their olivine hosts (12). In cases where Fe-Mg disequilibrium between a melt inclusion and its host olivine was evident, either equilibrium olivine or Fe^{2+} was added incrementally to each melt composition until equilibrium with the host olivine was achieved. On average, post-entrapment corrections resulted in $<8\%$ change in $\text{Fe}^{3+}/\Sigma\text{Fe}$ (table S2). Moreover, $\text{Fe}^{3+}/\Sigma\text{Fe}$ and H_2O measured on a MORB melt inclusion and the glass

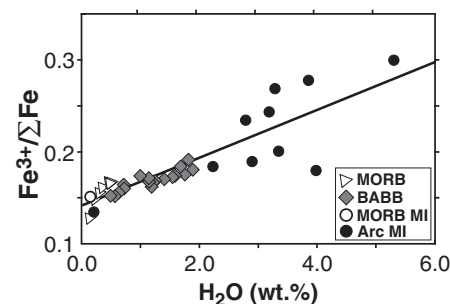


Fig. 3. Plot of measured H_2O concentrations versus $\text{Fe}^{3+}/\Sigma\text{Fe}$ determined by μ -XANES for MORB and BABB glasses, and olivine-hosted melt inclusions (MIs) from MORBs and global arc volcanoes. $\text{Fe}^{3+}/\Sigma\text{Fe}$ in MIs have been corrected for post-entrapment olivine crystallization or outward Fe^{2+} diffusion to place the melt compositions in equilibrium with the host olivine. Data for H_2O are published FTIR data from the literature or are FTIR or ion microprobe data from this study (12). Symbols exceed the size of the error bars in $\text{Fe}^{3+}/\Sigma\text{Fe}$ [± 0.0045 (1σ)]. The solid line is a least-squares linear regression through all of the data, with equation $y = 0.026x + 0.14$ [correlation coefficient (r^2) = 0.72]. When only MORB and BABB data are used, linear regression gives $y = 0.018 + 0.14$ ($r^2 = 0.65$).

exterior to its olivine host directly overlap, suggesting that processes specific to melt inclusions are not the primary cause of the trend.

Rather than shallow or sample-specific processes, melt oxidation appears to be linked to the composition of the mantle source, an idea that is supported by trace element variations. For example, the ratio of Ba concentration (an element that is highly mobile in aqueous fluids) to La concentration (an element that is fluid-immobile) is a proxy for the influence of slab-derived fluid on the composition of the sub-arc mantle source. In the basalt samples from the Mariana arc and back-arc basin, Ba/La ratios of lavas (12) progressively increase with increasing $\text{Fe}^{3+}/\Sigma\text{Fe}$ ratios (Fig. 4 and table S3). Because the Ba/La ratio is minimally influenced by magmatic processes, it is considered a true reflection of the mantle source that gave rise to a given basalt. Covariation of the Ba/La ratio with $\text{Fe}^{3+}/\Sigma\text{Fe}$ thus suggests that oxidation is directly related to the addition of H_2O from the subducted slab.

The relation between H_2O , trace elements sensitive to slab additions, and Fe oxidation state requires that slab-derived fluids be directly linked to the oxidation process. The slope of the observed trend in $\text{Fe}^{3+}/\Sigma\text{Fe}$ ratio versus H_2O concentration indicates the magnitude of magmatic oxidation associated with the addition of fluids from the subducted plate. A simple linear regression of the global data yields a slope of 0.026 (that is, basalt $\text{Fe}^{3+}/\Sigma\text{Fe}$ increases on average by this amount with each weight % increase in magmatic H_2O). Arc melt inclusion data show more variation relative to the tightly correlated MORB and BABB glasses, which internally give a slope of 0.018. The scatter in the arc data probably reflects the geographical diversity of the arc samples, because each volcano samples a distinct combination of slab characteristics (such as plate age or sediment pile) and mantle inputs. Differing extents of fractional crystallization will also create small variations in both H_2O concentration and $\text{Fe}^{3+}/\Sigma\text{Fe}$ ratio, but we emphasize that such variability is minor relative to the observed trend.

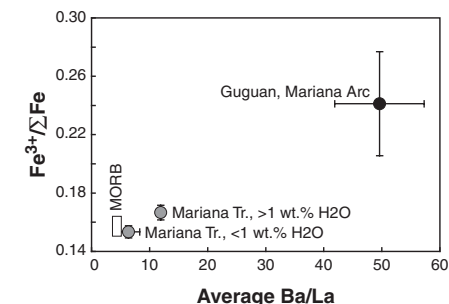


Fig. 4. Plot of average Ba/La ratio versus measured $\text{Fe}^{3+}/\Sigma\text{Fe}$ for MORBs, and subsets of BABB and arc basalts from the Mariana subduction zone. See supporting online material for sources of the Ba/La ranges for MORBs, the Guguan volcano, and the Mariana Trough. MORB and BABB glasses with 7.0 to 7.5 wt % MgO were used to average $\text{Fe}^{3+}/\Sigma\text{Fe}$.

Our data implicate the subduction process in the generation of magmas at higher oxygen fugacities than those of MORBs. If the mantle were equally reducing beneath ridges, back-arc basins, and arcs, then primitive undegassed basalts should have similar $\text{Fe}^{3+}/\Sigma\text{Fe}$ ratios in all three tectonic settings. At subduction zones, however, hydrated oxidized oceanic crust from Earth's surface is thrust into the mantle, where it contributes H_2O -rich fluids and/or melts, and its oxidized signature, to the mantle sources of arc volcanoes and back-arc spreading ridges (Fig. 1A). Indeed, undegassed BABBs and arc melts are systematically more oxidized than MORBs (Fig. 3). Differences between these tectonic regions may actually be underestimated, because H_2O acts to increase the extent of melting, leading to trace-element dilution at high melt fractions (11, 19). If Fe^{3+} behaves strictly as an incompatible element, $\text{Fe}^{3+}/\Sigma\text{Fe}$ is expected to be higher in MORBs, where melt fractions are low, and to be lower in BABBs and arc basalts, where melt fractions are higher. On the other hand, H_2O may lower the activity coefficient of FeO during mantle melting, which could increase $\text{Fe}^{3+}/\Sigma\text{Fe}$ in hydrous mantle melts (11, 20, 21); however, experimental studies are not conclusive (21, 22) and the effect of H_2O is likely to be minor relative to that of temperature (21).

Although H_2O concentrations and the oxidation state of Fe correlate linearly in these basalts, H_2O is not required to be the cause of oxidation. Water acts as an efficient oxidizing agent in many terrestrial environments, but not in Earth's upper mantle (23). For H_2O alone to play this role requires the efficient dissociation of H_2 from O^{2-} , followed by the efficient removal of H_2 . Magmatic oxidation due to loss of H_2 may be responsible for oxidizing basalt pillow cores (8) at low pressure, but whether H_2O can dissociate to liberate H_2 in the mantle wedge remains controversial (18, 23). The relation between Fe oxidation state and magmatic H_2O content at subduction zones may instead arise indirectly, as a consequence of the oxidized condition of the subducted oceanic lithosphere. Iron in marine sediments is highly oxidized [$\text{Fe}^{3+}/\Sigma\text{Fe} = \sim 82\%$ (2)], and hydrothermal alteration of both basalt and peridotite results in a net oxidation of the oceanic lithosphere through the formation of Fe-oxyhydroxides and magnetite and the release of H_2 to the ocean (2, 24). The subducting plate thus enters the mantle at intrinsically higher oxygen fugacity and clearly supplies the H_2O flux into the mantle wedge, but the associated transfer of the oxidized signature from the slab is poorly understood.

Dilute aqueous fluids are inefficient carriers of Fe^{3+} (25), but as slab-derived components become more acidic, more saline, or more melt-like, Fe^{3+} may become highly mobile, as has been shown for other trivalent fluid-immobile elements (26, 27). Transporting all of the Fe^{3+} that we observe in arc basalts in excess of MORBs directly from the slab into the mantle wedge would therefore require that slab-derived H_2O -rich components be hypersaline brines, supercritical fluids, or

silicate melts of subducted sediments or the basaltic plate (26–28). Alternatively, fluid-mobile elements such as S could oxidize the mantle wedge of subduction zones without requiring direct transport of Fe^{3+} . If the intrinsic oxygen fugacity of fluids released from the descending slab is sufficiently high to carry S as sulfate (S^{6+}), then 1 mol of S has the potential to oxidize 8 mol of Fe^{2+} as sulfate in the fluid is reduced to form sulfide (S^{2-}) in the mantle. Sulfur reduction will take place provided that the oxygen fugacity of the mantle wedge remains below the sulfur-sulfur oxide buffer, or approximately QFM + 2 (29). From this perspective, if hydrous slab-derived components carry sufficient sulfate (30), direct addition of Fe^{3+} from the slab may not be required.

References and Notes

1. B. J. Wood, L. T. Bryndzia, K. E. Johnson, *Science* **248**, 337 (1990).
2. C. Lecuyer, Y. Ricard, *Earth Planet. Sci. Lett.* **165**, 197 (1999).
3. C.-T. A. Lee, W. P. Leeman, D. Canil, Z.-X. A. Li, *J. Petrol.* **46**, 2313 (2005).
4. D. Canil, *Earth Planet. Sci. Lett.* **195**, 75 (2002).
5. A. J. Berry, L. V. Danyushevsky, H. S. C. O'Neill, M. Newville, S. R. Sutton, *Nature* **455**, 960 (2008).
6. I. J. Parkinson, R. J. Arculus, *Chem. Geol.* **160**, 409 (1999).
7. V. C. Kress, I. S. E. Carmichael, *Contrib. Mineral. Petrol.* **108**, 82 (1991).
8. D. M. Christie, I. S. E. Carmichael, *Earth Planet. Sci. Lett.* **79**, 397 (1986).
9. M. Sato, T. L. Wright, *Science* **153**, 1103 (1966).
10. J. F. Luhr, *Contrib. Mineral. Petrol.* **142**, 261 (2001).
11. E. Stolper, S. Newman, *Earth Planet. Sci. Lett.* **121**, 293 (1994).
12. Materials and methods are available as supporting material on Science Online.
13. M. Wilke, G. M. Partzsch, R. Bernhardt, D. Lattard, *Chem. Geol.* **220**, 143 (2005).
14. E. Cottrell, K. A. Kelley, A. T. Lanzirotti, R. A. Fischer, *Chem. Geol.*, in press.
15. R. E. Botcharnikov, J. Koepke, F. Holtz, C. McCammon, M. Wilke, *Geochim. Cosmochim. Acta* **69**, 5071 (2005).
16. E. Hauri, *Chem. Geol.* **183**, 99 (2002).
17. T. W. Sisson, S. Bronto, *Nature* **391**, 883 (1998).

18. A. D. Brandon, D. S. Draper, *Geochim. Cosmochim. Acta* **62**, 333 (1998).
19. K. A. Kelley et al., *J. Geophys. Res.* **111**, B09208 (2006).
20. I. Kushiro, *J. Petrol.* **13**, 311 (1972).
21. G. A. Gaetani, T. L. Grove, *Contrib. Mineral. Petrol.* **131**, 323 (1998).
22. K. Hirose, T. Kawamoto, *Earth Planet. Sci. Lett.* **133**, 463 (1995).
23. B. R. Frost, C. Ballhaus, *Geochim. Cosmochim. Acta* **62**, 329 (1998).
24. M. E. Berndt, D. E. Allen, W. E. Seyfried, *Geology* **24**, 351 (1996).
25. M. E. Schneider, D. H. Eggler, *Geochim. Cosmochim. Acta* **50**, 711 (1986).
26. M. C. Johnson, T. Plank, *Geochem. Geophys. Geosyst.* **1**, 10.1029/1999GC000014 (1999).
27. R. Kessel, M. W. Schmidt, P. Ulmer, T. Pettke, *Nature* **437**, 724 (2005).
28. C. E. Manning, *Earth Planet. Sci. Lett.* **223**, 1 (2004).
29. M. R. Carroll, M. J. Rutherford, *J. Petrol.* **28**, 781 (1987).
30. P. J. Wallace, *J. Volcanol. Geotherm. Res.* **140**, 217 (2005).
31. Thanks to R. Fischer and D. Kratzmann for beamline assistance and data processing; T. Gooding for sample preparation; A. Logan for electron microprobe assistance; D. Christie, T. Plank, L. Cooper, M. Zimmer, E. Hauri, M. Hirschmann, and C. Langmuir for samples, data, and discussion; and A. Lanzirotti for beamline method development. This work was supported by a Smithsonian Scholarly Studies Grant to E.C., a NSF ADVANCE fellowship to K.K., and NSF awards EAR-0841108 (K.K.) and EAR-0841006 (E.C.). NSF award OCE-0644625 provided curatorial support for marine geological samples at the University of Rhode Island. Beamline X26A is supported by the U.S. Department of Energy (DOE) Geosciences Division (grant DE-FG02-92ER14244 to the University of Chicago, Consortium for Advanced Radiation Sources). Use of the National Synchrotron Light Source was supported by DOE under contract no. DE-AC02-98CH10886.

Supporting Online Material

www.sciencemag.org/cgi/content/full/325/5940/605/DC1
Materials and Methods
Figs. S1 to S4
Tables S1 to S3
References

27 March 2009; accepted 10 June 2009
10.1126/science.1174156

The cAMP Sensor Epac2 Is a Direct Target of Antidiabetic Sulfonylurea Drugs

Chang-Liang Zhang,¹ Megumi Katoh,¹ Tadao Shibasaki,¹ Kohtaro Minami,¹ Yasuhiro Sunaga,^{1*} Harumi Takahashi,¹ Norihide Yokoi,¹ Masahiro Iwasaki,¹ Takashi Miki,¹ Susumu Seino^{1,2,3,†}

Epac2, a guanine nucleotide exchange factor for the small guanosine triphosphatase Rap1, is activated by adenosine 3',5'-monophosphate. Fluorescence resonance energy transfer and binding experiments revealed that sulfonylureas, widely used antidiabetic drugs, interact directly with Epac2. Sulfonylureas activated Rap1 specifically through Epac2. Sulfonylurea-stimulated insulin secretion was reduced both in vitro and in vivo in mice lacking Epac2, and the glucose-lowering effect of the sulfonylurea tolbutamide was decreased in these mice. Epac2 thus contributes to the effect of sulfonylureas to promote insulin secretion. Because Epac2 is also required for the action of incretins, gut hormones crucial for potentiating insulin secretion, it may be a promising target for antidiabetic drug development.

Epac is a guanine nucleotide exchange factor (GEF) for the Ras-like small guanosine triphosphatases Rap1 and Rap2 that is activated by the direct binding of adenosine

3',5'-monophosphate (cAMP); two isoforms of Epac (also referred to as cAMP-GEF), Epac1 (cAMP-GEF1) and Epac2 (cAMP-GEF2), have been identified (1–4). Epac2 mediates the potentiation of